Supplementary information for:
"Drying dip-coated colloidal films"

Joaquim Li, Bernard Cabane, Michael Sztucki, Jérémie Gummel, Lucas Goehring

Calibration of the peak positions

In order to calibrate the relation between the position of the peak in the structure factor q_{peak} and the silica volume fraction ϕ_s, we used a series of dispersions obtained through dialysis with aqueous solutions of PEG 35000 (see Materials and Methods). We measured q_{peak} and ϕ_s in each one. This calibration does not depend on any assumptions regarding the sizes or the ordering of the silica particles, provided that the short-range order is determined by ϕ_s only. We then found that $(q_{peak})^3$ is proportional to ϕ_s, in the range (0.03 – 0.5), as it should for repelling particles (Figure SI-1) [1]. Moreover, this relation of proportionality can be modelled by treating the system as a face-centered cubic array of particles with a number-averaged radius R_p = 8.15 nm [1]

$$\left(q_{peak}\right)^3 = \left(\frac{2\pi}{d_{111}}\right)^3 = \frac{36\pi^2\sqrt{3}}{\left(2R_p\right)^3}\phi_s \text{ with } \quad d_{111} = \left(\frac{16\pi}{3\phi_s}\right)^{1/3}\frac{R_p}{\sqrt{3}} \qquad \text{/SI-1/}$$

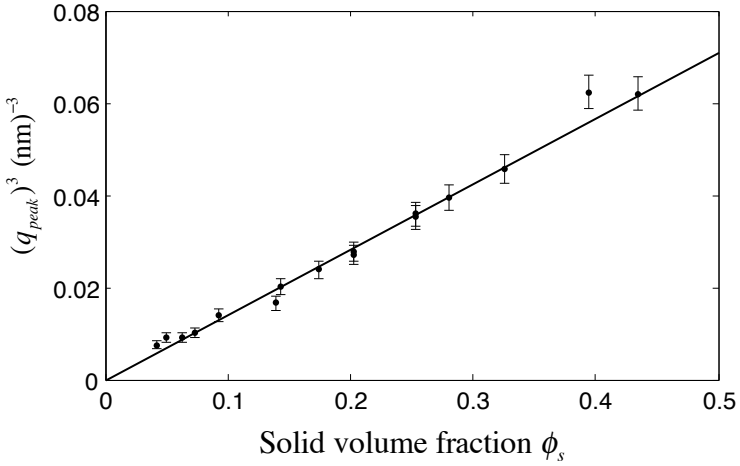

Figure SI-1. The relation between the position of the first peak of the structure factor and the volume fraction of silica particles in the dispersion. Two series of concentrated dispersions were prepared separately, and both gave the same calibration curve, with a coefficient of proportionality of 0.142 ± 0.03 nm^{-3}, as shown.

Determination of the integral of the scattered intensity

At high q values, the integral of the intensity scattered in all directions of reciprocal space goes to a limit (Qh) that depends only on the average fluctuation of the density of scattering length in the volume that is irradiated by the beam. For materials that have only 2 levels of the density of scattering length, this average fluctuation is expressed simply as a function of this difference in scattering density, and of the volume fraction of these two phases

$$Qh = \int_0^\infty I_{exp}(q)\, q^2 dq = 2\pi^2 h \phi_s \Delta\rho^2 \left(1-\phi_s\right) \qquad \text{/SI-2/}$$

The SAXS experiment does not reach infinite q values; therefore, we have measured the values of Qh at finite q_{max} values. Fig. SI-2 shows how Qh varies with q_{max} for a selection of spectra recorded during the drying of a film. We see that, due to the low signal / noise ratio at high q, the value of Qh fluctuates considerably for values of q_{max} that are beyond 3 nm^{-1}. Such q values correspond to distances below 3 nm, which are intra- rather than inter-particle distances. We take advantage of this fact to overcome the signal/noise problem.

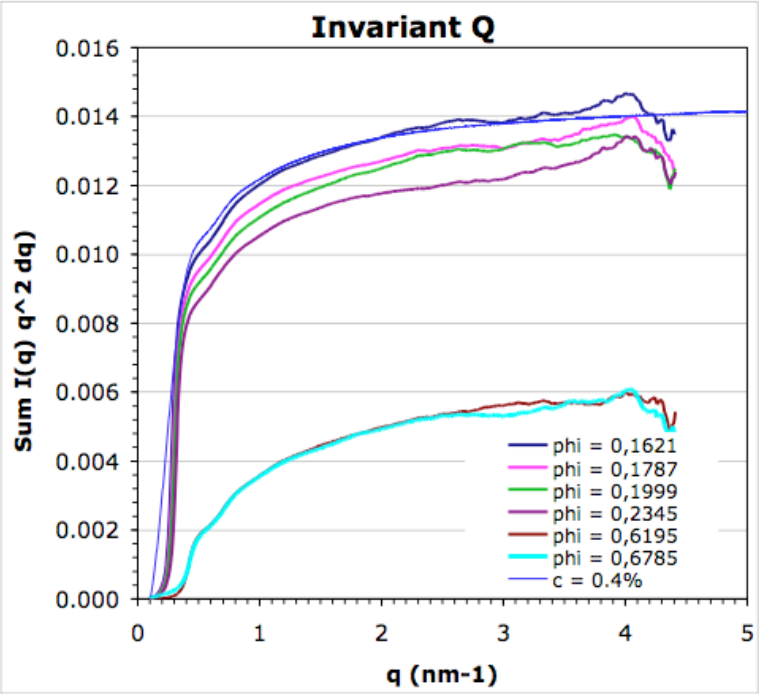

Figure SI-2. The integral of the scattered intensity of the film as a function of the highest value of q used for the integration. The line that extends beyond q = 4.5 nm^{-1} is the corresponding integral for a dilute dispersion, using a scale factor that matches both sets of data at q = 3 nm^{-1}.

In order to obtain more accurate values of Qh, we used a spectrum recorded independently for a thick (h = 1 mm) sample of a dilute ($\phi_s = 4 \times 10^{-3}$) dispersion of the same colloidal silica. For this spectrum, we had a better signal over noise ratio that allowed us to calculate an accurate value of Qh, taking q_{max} = 5 nm^{-1} (Fig. SI-3). We note that the asymptotic limit of the scattering from the dilute dispersion is approximately 10% higher than that of polydisperse spheres with the same average radius (Fig. SI-3). This is because the individual silica particles have non-spherical surfaces, as shown by transmission electron microscopy [2].

Since the particles in the dilute dispersions and those in the films were the same, and since they are incompressible, we spliced the data from a dilute dispersion and from the films to obtain SAXS curves that matched the film data at all q values corresponding to inter-particle distances (q < 3 nm^{-1}) but had better signal ratio for distances that were well within a particle (q> 3 nm^{-1}). These spliced curves were then used to calculate the value of Qh.

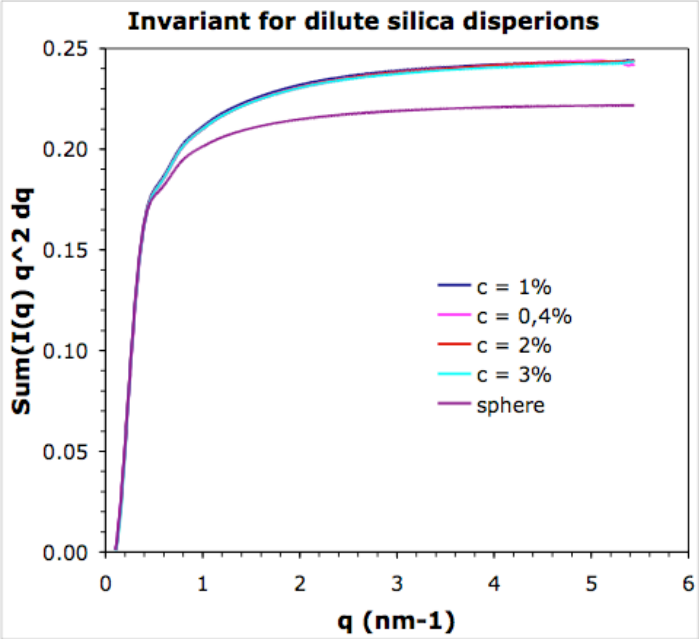

Figure SI-3. The integral of the scattered intensity as a function of the highest value of q used in the integration, for dilute dispersions of Ludox HS-40 colloidal silica, compared with the theoretical limit for polydisperse spheres with a Schulz distribution of radii, as defined in the main text, Fig. 4. All intensities have been normalized to that given by a dispersion of concentration $\phi_s = 1 \times 10^{-2}$.

Determination of the Porod limit of the scattered intensity

At high q values, materials that have only two levels of the density of scattering length follow Porod's law, which is a q^{-4} decay of the intensity. The prefactor of this power law, also called the Porod limit, is determined by the total area of interface between the two phases of the material, as expressed in Eqn. /SI-3/ (corresponding to Eqn. /6/ of the main text).

$$\lim_{q\to\infty} q^4 I_{exp}(q) = 2\pi h \phi_s \Delta\rho^2 \frac{A_p}{V_p} \qquad \text{/SI-3/}$$

In order to determine this limit, we used the classical plot of $I(q)$ vs. q^{-4}: the prefactor of the power law is the initial slope of this plot, and the ordinate at the origin is a background correction.

Fig. SI-4 shows an example of this type of plot for a thick sample (h = 1 mm) of a dilute dispersion of the same colloidal silica ($\phi_s = 4 \times 10^{-3}$). These plots are compared with the theoretical plot for a Schulz distribution of spheres with a mean radius R_p = 8.0 nm and width σ_R/R_p=0.14. As seen in Fig. SI-2, the Porod limit of the Ludox HS-40 particles is higher than that of the corresponding spheres, because the particles are somewhat aspherical.

Using the plot shown in Fig. SI-4, which yields a Porod limit $q^4 I(q) = 1.68 \times 10^{34}$ m^{-4}, together with Qh for the same dispersion, $Qh = 8.91 \times 10^{25}$ m, a difference in density of scattering length $\Delta\rho^2 = 5.69 \times 10^{29}$ m^{-2}, and a volume fraction $\phi_s = 4 \times 10^{-3}$, we obtained a surface area per unit volume $A_p/V_p = 5.90 \times 10^8$ m^{-1} through Eqn. SI-4:

$$\frac{\lim_{q\to\infty} q^4 I_{exp}(q)}{Qh} = \frac{A_p}{V_p} \times \frac{1}{\pi(1-\phi_s)} \qquad \text{/SI-4/}$$

This surface area per unit volume corresponds to an area per unit mass $A_p/M_p = 2.68 \times 10^5$ m^2kg^{-1}, slightly higher than that provided by the manufacturer from BET measurements ($A_p/M_p = 2.20 \times 10^5$ m^2kg^{-1}).

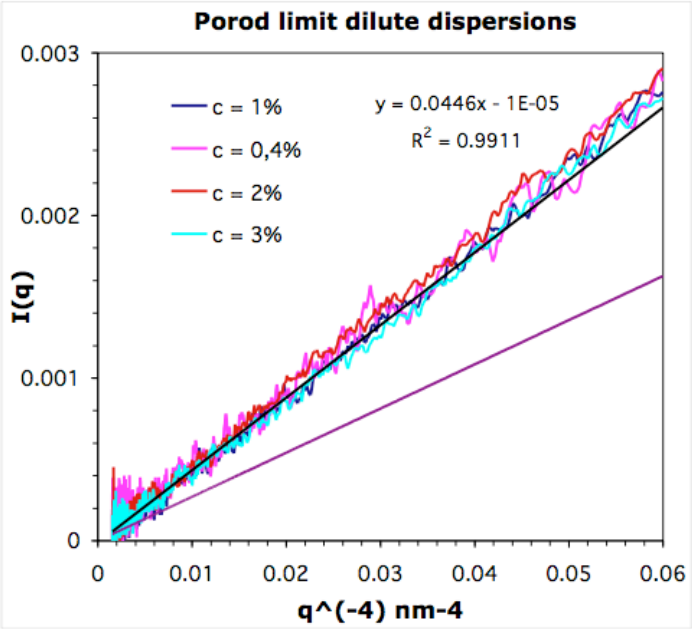

Figure SI-4. The Porod limit of dilute dispersions of Ludox HS-40 colloidal silica, compared with the theoretical limit for a Schulz distribution of spheres with the same average radius. All intensities have been normalized to that given by a dispersion of concentration $\phi_s = 1 \times 10^{-2}$.

Fig. SI-5 shows the Porod plots for a selection of spectra recorded during the film drying experiment. Because these spectra have a low signal-to-noise ratio at high q, the accuracy on the initial slope on the Porod plots is poor. Consequently, we have determined this slope using an extended range of q (from q = 1.2 to 3.2 nm^{-1}). This results in systematically underestimated slopes. As in the case of the invariant, we can use the comparison with the scattering from bulk samples to evaluate the required correction.

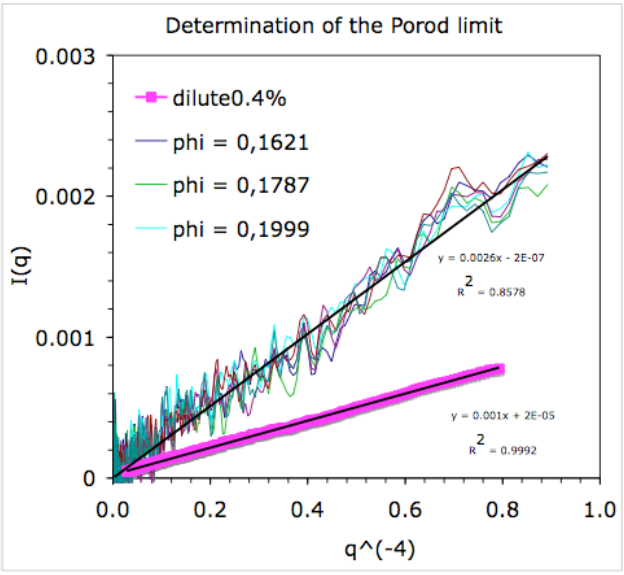

Figure SI-5. The Porod limit of dilute films of Ludox HS-40 colloidal silica, compared with that for dilute dispersions of the same colloidal silica.

Indeed, the distances probed by the experiment in this range of q values extend from $d = 2\pi/q$ = 2 to 5 nm. These distances are essentially intraparticle rather than interparticle distances. Accordingly, we assumed that the variations of the Porod limit at very high q values were the same for the drying films and for bulk samples of dilute silica dispersions. The slopes of the Porod plots given in Fig. SI-6 shows that this is true within experimental uncertainties. Accordingly, based on the evolution of the slope of the Porod plot with changes in the q^{-4} range used, the Porod limit determined for films in the range extending to $q^{-4} = 0.5$ nm^4 was only 80 % of the true asymptotic Porod limit (asymptotic value 2.9×10^{-3} nm^{-4} rather than 2.35×10^{-3} as seen in Fig. 8 of the main text).

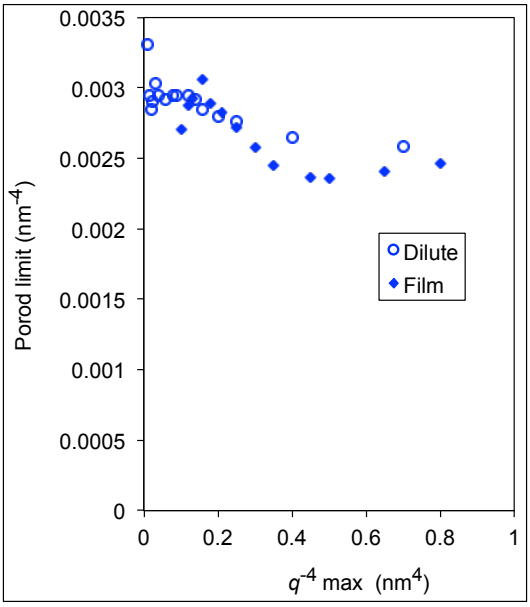

Figure SI-6. Evolution of the initial slope of the Porod plot depending on the q range considered for the determination of the slope. Horizontal scale: highest value of q^{-4} used in the determination of the slope of the Porod plot. Full diamonds are the data obtained for a thick sample of a dilute dispersion of ludox HS-40 colloidal silica, scaled to match the average level of the film data. Empty circles are an average over time of the data obtained for the spectra recorded during the drying film experiment.

Agreement between the absolute values of the volume fraction, Porod limit and the integral of the scattered intensity

One can obtain values of $h\phi_s$ from the fit of the evolution of Qh by Eqn. /11/ in the main text

$$h\phi_s = \frac{K}{2\pi^2 \Delta\rho^2} \qquad /SI\text{-}5/$$

as well as the from the value of the Porod limit

$$h\phi_s = \frac{\lim_{q\to\infty} q^4 I_{\exp}(q)}{2\pi\Delta\rho^2 \frac{A_p}{V_p}} \qquad /SI\text{-}6/$$

By combining Eqns. SI-5 and SI-6 we obtain

$$\lim_{q\to\infty} q^4 I_{\exp}(q) = \frac{K}{\pi}\frac{A_p}{V_p} \qquad /SI\text{-}7/$$

In order to check the consistency of our measurements, we need an estimate of the ratio A_p/V_p. Such a ratio has been obtained from Eqn. SI-4. We obtained $A_p/V_p = 5.90 \times 10^8$ m^{-1}. Using this value for A_p/V_p and $K = 1.61 \times 10^{-2}$ nm^{-3} one finds a Porod limit of 3.0×10^{-3} nm^{-4}. This is in agreement with the trends shown in Fig. SI-6.

The integral of the scattered intensity for systems with either 2 or 3 constant levels of scattering density

Consider a material described by its electronic density, $\rho(\vec{r})$. This density has an average value, $\langle\rho(\vec{r})\rangle$, and its spatial fluctuations around the average value are described by $\eta(\vec{r})$:

$$\eta(\vec{r}) = \rho(\vec{r}) - \langle\rho(\vec{r})\rangle \qquad \text{/SI-8/}$$

The scattered amplitude is a Fourier transform of $\eta(\vec{r})$, and the scattered intensity is proportional to the average squared fluctuation $\langle\eta^2(\vec{r})\rangle$. The integral over all $\vec{q}$ vectors of the scattered intensity (also called the invariant) is [3,4]:

$$Qh = \int_0^\infty I_{exp}(q)\, q^2\, dq = 2\pi^2 h \langle\eta^2\rangle \qquad \text{/SI-9/}$$

In a system with only 2 levels of electron density, with some volume fraction ϕ_w of water with an electron density ρ_w, and volume fraction ϕ_s of silica with an electron density ρ_s, the average density $\rho(\vec{r}) = \rho_w\phi_w + \rho_s\phi_s$. In regions of water, the squared fluctuation is

$$\eta_w^2 = (\rho_w - (\rho_w\phi_w + \rho_s\phi_s))^2 \qquad \text{/SI-10/}$$

with a similar expression for η_s^2. The average squared fluctuation is the sum of the squared fluctuations in both types of regions, $\langle\eta_{wet}^2\rangle = \eta_w^2\phi_w + \eta_s^2\phi_s$, which simplifies to the classical expression

$$\langle\eta_{wet}^2\rangle = (\rho_w - \rho_s)^2\,\phi_w\phi_s = (\rho_w - \rho_s)^2\,\phi_s(1-\phi_s) \qquad \text{/SI-11/}$$

For a three-phase system, if some regions are filled with air of an electron density ρ_0, and volume fraction ϕ_0, the new total average electron density is $\langle\rho(\vec{r})\rangle = \rho_0\phi_0 + \rho_w\phi_w + \rho_s\phi_s$, and thus, for example,

$$\eta_w^2(\vec{r}) = \left[\rho_w(\vec{r}) - (\rho_0\phi_0 + \rho_w\phi_w + \rho_s\phi_s)\right]^2 \qquad \text{/SI-12/}$$

The average squared fluctuation is now the sum of the squared fluctuations in all 3 types of regions:

$$\langle\eta_{dry}^2\rangle = \eta_0^2\phi_0 + \eta_w^2\phi_w + \eta_s^2\phi_s$$

$$= \rho_0^2\phi_0(\phi_w+\phi_s) + \rho_w^2\phi_w(\phi_0+\phi_s) + \rho_s^2\phi_s(\phi_0+\phi_w) - 2\rho_0\rho_w\phi_0\phi_w - 2\rho_0\rho_s\phi_0\phi_s - 2\rho_w\rho_s\phi_w\phi_s \qquad \text{/SI-13/}$$

which simplifies to

$$\langle\eta_{dry}^2\rangle = (\rho_0 - \rho_w)^2\,\phi_0\phi_w + (\rho_w - \rho_s)^2\,\phi_w\phi_s + (\rho_s - \rho_0)^2\,\phi_s\phi_0 \qquad \text{/SI-14/}$$

We have measured the integral of the scattered intensity in the wet and in the dry solid. Therefore we can determine ϕ_w and ϕ_0 through the ratio

$$\frac{\langle \eta_{dry}^2 \rangle}{\langle \eta_{wet}^2 \rangle} = \frac{Q_{dry}}{Q_{wet}} \qquad \text{/SI-15/}$$

and the relation $\phi_w + \phi_s + \phi_0 = 1$. A resolution of Equation /SI-15/ with $(\rho_w - \rho_s)^2 = 5.69 \times 10^{29}$, $(\rho_s - \rho_0)^2 = 2.88 \times 10^{30}$, $(\rho_w - \rho_0)^2 = 8.89 \times 10^{29}$, $\phi_2 = 0.68$ and $Q_{dry}/Q_{wet} = 3.2$ yields an air volume fraction $\phi_0 = 0.16$ and a water volume fraction $\phi_w = 0.16$. This residual water content corresponds to 1-2 molecular layers of water on the silica particles, assuming that a dense molecular layer of water has a thickness of 0.3×10^{-9} m. This amount of residual water is what is expected at ambient relative humidity (RH = 50 %) [5].

Final film thickness

In order to find out whether the drying process produced uniform solid films, we performed a SAXS scan of a fully dried dip-coating film along its length (i.e. along the dip-coating direction). Figure SI-7 presents the measured values of the invariant of the scattered intensity and the values of the silica volume fraction, calculated from the position of the first peak of the structure factor. The values of the invariant have been scaled by a constant factor (1/21) in order to facilitate the comparison with the silica volume fraction. Both sets of data indicate that the film is nearly uniform, with a variation of 5% over the central part of the film (positions 5000 to 15000 µm). However, there are significant excesses of deposited silica at both ends of the film, particularly at the bottom end where a bulge of liquid dispersion remained at the end of the dip-coating. We can also note an increase in silica volume fraction at the bulges [6].

After the SAXS experiment was completed, we scanned the film again, using a white light reflectometer to determine the film thickness. For this determination we used the index of refraction of mica (approximated by that of BK7 glass), and that of water. This scan confirmed that the film thickness was uniform, excepted for the bulges at both ends of the film (Figure SI-7). The average film thickness measured in this way (taking the mean value between position 5 mm and 15 mm) was $h = 1.6$ µm, compared with that determined through the SAXS invariant, which was $h = 2.1$ µm

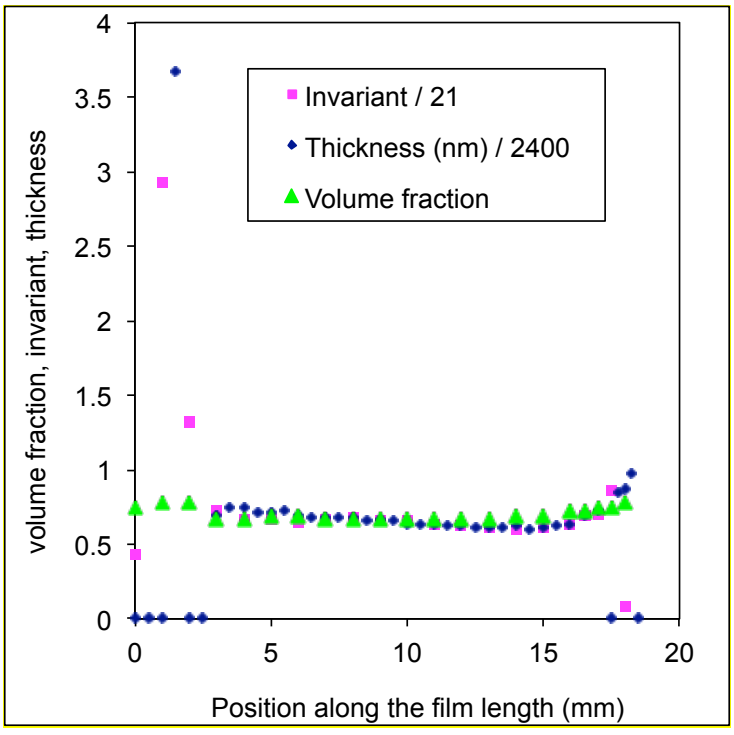

Figure SI-7. Scans through a dry film, along the direction of dip-coating. The horizontal scale goes from 0 (top of the deposited film) to 20 mm (bottom of the mica). Green triangles: Volume fraction of silica, calculated from the position of the first peak of the structure factor. Pink squares: invariant of the scattered intensity, in nm^{-3}, scaled by 1/21. Blue diamonds: thickness of the film, in µm, scaled by 1/2.4. The average film thickness was 2 µm.

References

1 Goodwin, J.W.; Ottewill, R.H.; Parentich, A. *J. Phys. Chem*. **1980**, *84*, 1580.

2 Madeline, J. B.; Meireles, M.; Bourgerette, C.; Botet, R.; Schweins, R.; Cabane, B. *Langmuir* **23**, 1645, (2007).

3 Spalla, O. in *Neutrons, X-rays and light: scattering methods applied to soft condensed matter*; chapter 3, P. Lindner and T. Zemb Eds., North Holland **2002**.

4 Glatter, O.; Kratky, O. *Small Angle X-ray scattering*; Academic Press: London 1982.

5 Asay, D.B. ; Kim, S.H. *J. Phys. Chem. B* **2005**, *109*, 16760

6 Marin, A.G. ; Gelderblom, H. ; Lohse, D. ; Snoeijer, J.H. *Phys. Rev. Lett.* **2011**, 107, 085502